SIMULATIONS AND EXPERIMENTS OF BEAM-BEAM EFFECTS IN e^+e^- STORAGE RINGS *

Y. Cai[†], J. Seeman, SLAC, Menlo Park, CA 94025, USA
W. Kozanecki, CEA/DSM/DAPNIA, Gif-sur-Yvette, France
K. Ohmi, M. Tawada, KEK, 1-1 Oho, Tsukuba, 305-0801, Japan

Abstract

Over the past decade, extensive simulations of beam-beam effects in e^+e^- colliders, based on the particle-in-cell (PIC) method, were developed to explain many complex experimental observations. Recently, such simulations were used to predict the future luminosity performance of e^+e^- colliders. Some predictions have been proven to be correct in the existing accelerators. In this paper, many effects such as the beam-beam limit, crossing angle, parasitic collisions, betatron spectrum, and the beam-beam lifetime, will be directly compared between simulations and experiments.

INTRODUCTION

In addition to incoherent resonances, the colliding beams can also be excited by coherent resonances. To study these coherent modes, a strong-strong model for two-dimensional round beams was first introduced by Krishnagopal and Siemann [1]. Later, the simulation was extended to flat beams [2, 3] and recently [4], to three-dimensional beams using parallel computing [5]. The strong-strong model of the beam-beam interaction is self-consistent and has achieved numerical convergence within the accuracy required for luminosity calculation.

Luminosity

The luminosity, defined as the interaction rate per unit cross section, is the most important parameter that measures the performance of a collider. It can be calculated as an overlapping integral of the distributions of the colliding bunches. For infinite short bunches with Gaussian distributions, it can be written as

$$L_b = \frac{N_+N_-f_0}{2\pi\sqrt{(\sigma_{x,+}^{*2} + \sigma_{x,-}^{*2})(\sigma_{y,+}^{*2} + \sigma_{y,-}^{*2})}}, \quad (1)$$

where f_0 is the revolution frequency, $N_{+,-}$ are the bunch populations, and $\sigma_{x,y}^*$ are the beam sizes at the interaction point (IP). Subscripts + and - denote the positron or electron respectively.

Beam-beam limit

Based on the Bassetti and Erskine formula [6], the beam-beam force is linearly focusing near the center of the beam. The tune shift, generated by the linear focusing, is described by the beam-beam parameters:

$$\xi_{y,\pm} = \frac{r_e N_\mp \beta_{y,\pm}^*}{2\pi\gamma_\pm\sigma_{y,\mp}^*(\sigma_{x,\mp}^* + \sigma_{y,\mp}^*)}, \quad (2)$$

where r_e is the classical radius of the electron, β_y^* is the vertical beta function at the IP, and γ is the relativistic factor. Most importantly, this parameter also characterizes the size of the beam footprint in the tune plane. Given a working point, its nearby space is limited by the surrounding incoherent and coherent resonances. As a result, this parameter is always limited. This is call the beam-beam limit.

For simplicity, assume that $\sigma_{x,+}^* = \sigma_{x,-}^*$, $\sigma_{y,+}^* = \sigma_{y,-}^*$ and that both beams are very flat. The luminosity can be rewritten in terms of the beam-beam parameter as

$$L_b \approx \frac{N_\pm\gamma_\pm f_0 \xi_{y,\pm}}{2r_e\beta_{y,\pm}^*}. \quad (3)$$

This formula is often used for estimating the luminosity of e^+e^- colliders, assuming empirically a certain beam-beam limit, say $\xi_{y,\pm} = 0.05$.

However in realistic asymmetric colliders, assumptions, such as Gaussian distributions or equal beam sizes, are often invalid. In addition, there are more beam-beam effects, such as the crossing angle and parasitic collisions, that make a self-consistent simulation necessary in order to calculate the luminosity in these colliders.

In this paper, we directly compare simulations with measurements. First, we briefly review the PIC method. Second, we compare luminosity related measurements with simulations. Finally we show the beam-beam lifetime calculation with a nonlinear map representing the machine lattice. Due to limited space, only the PEP-II results are shown and the crossing angle measurements are refer to another paper [7] in these proceedings.

SIMULATION METHOD

In a strong-strong model of beam-beam simulation, both beams are represented by macro particles. The profile of macro particles is retained in every step during the simulation. A bunch is divided into several longitudinal slices and each slice contains many macro particles. The position of the slices is chosen such that the number of macro

particles in every slice is approximately the same. The collision is calculated for every pair of colliding slices in the appropriate time sequence.

For each pair of colliding slices, the transverse positions of macro particles are used to construct the charge distribution on a rectangular grid at the actual collision point. In our simulation, a typical mesh is 128×128 and it is divided into 10 grid points per sigma in the horizontal plane and 5 in the vertical plane. This choice for the mesh, together with 160,000 macro particles divided into five slices, is adequate to achieve numerical convergence of the luminosity.

The charge distribution on the grid is then used to obtain the potential by solving Poisson's equation with an inhomogeneous boundary condition [3]. The electric field on the grid is derived as the gradient of the potential. Given the transverse position of an incoming particle, the field value at that position, in general off the grid, is computed by interpolation from the field on the nearby grid points. The interpolated field is used to kick the incoming particle.

The longitudinal position of a particle is also used to interpolate the field value from the two boundaries of the slice to which the particle belongs. Besides the beam-beam collision, a six-dimensional linear map, radiation damping, and quantum excitations are included for the arcs in the simulation. The simulations are carried out on a PC cluster using 32 processors. For a typical run, a few damping times are required to reach equilibrium. That takes about eight hours.

NOMINAL CONDITIONS

PEP-II is an asymmetric B-factory that consists of two separate storage rings with different energies. The positron and electron beams are brought to the interaction point inside the BaBar detector for head-on collisions. The main parameters that relate to the beam-beam interaction are listed in Table 1. Most values in the table are based on the measurements; a few are derived from optical calculation. Unless specifically mentioned, these parameters are the input to the simulations in this paper.

In addition to the main collision, which is handled by the PIC method, we add the parasitic collisions at the two nearest crossing points as illustrated in Fig 1. The Gaussian approximation is used for these parasitic collisions and the beam sizes are updated every 1000 turns. Currently, PEP-II is operated with bunch spacing $s_b = 2s_{RF}$. The nominal beam separation $\Delta x = 3.22$ mm is about $11\sigma_x^-$ or $24\sigma_x^+$ at the crossing points.

Blow-up

Twelve simulations including parasitic collisions were carried out at different bunch populations ranging from 10% to 120% of the peak operating populations in Table 1. The ratio of the positron and electron currents are kept constant in the simulations. The results of the simulation are compared with different measurements in this section.

Table 1: PEP-II Main Parameters, Feb. 3, 2004

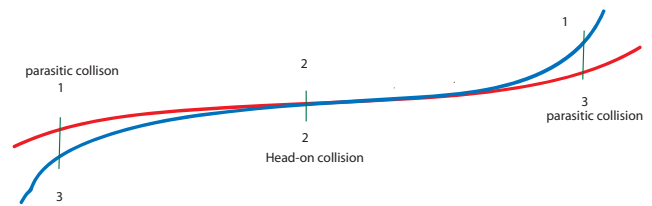| Parameter	LER (e+)	HER (e-)
beam energy E (Gev)	3.1	9.0
bunch population N	7.15×10^{10}	4.41×10^{10}
x beta at the IP β_x (cm)	50.0	27.0
y beta at the IP β_y (cm)	1.05	1.11
x emittance ϵ_x (nm-rad)	22.0	59.0
y emittance ϵ_y (nm-rad)	1.40	2.33
x tune ν_x	38.5162	24.5203
y tune ν_y	36.5639	23.6223
synchrotron tune ν_s	0.027	0.0495
bunch length σ_z (cm)	1.05	1.16
energy spread σ_δ	6.5×10^{-4}	6.1×10^{-4}
x,y damping τ_t (turns)	9800	5030
z damping τ_z (turns)	4800	2573

Figure 1: Parasitic collisions along with the head-on collision.

The equilibrium beam sizes as a function of the product of beam currents are shown in Fig. 2. The vertical blow-up of the electron beam is nearly 40% at the peak operating currents. That is consistent with the observation at the synchrotron light monitor. The horizontal luminous spot size $\sigma_x^l = \sigma_{x,+}^* \sigma_{x,-}^* / \sqrt{\sigma_{x,+}^{*2} + \sigma_{x,-}^{*2}}$ varies little and saturates at 68 μm. Similar results were obtained from the measurement using the BABAR detector [8]. The agreement is within a few percent.
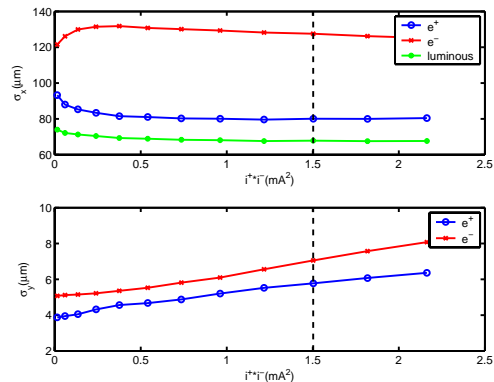

Figure 2: Simulated equilibrium beam sizes as a function of the product of beam currents. The dashed lines mark the product of peak operating currents.

Luminosity scan

Using a fast luminosity monitor, we measure the transverse beam size by measuring the luminosity while moving the electron beam across the positron beam. We then fit the luminosity with a Gaussian distribution of Σ_y. On the other hand, Σ_y can also be calculated, $\Sigma_y = \sqrt{\sigma_{y,+}^{*2} + \sigma_{y,-}^{*2}}$, using the equilibrium beam sizes in the simulation at 10% of the peak operating currents. Similar measurements were also performed in the horizontal plane. The results are summarized in Table 2.

Table 2: Luminosity scan at low beam currents. Measured on Feb. 10, 2004.

	Σ_x	Σ_y
simulation	153 μm	6.38 μm
measurement	146 μm	6.92 μm

Beam-beam parameter

In Fig 3 and Fig 4, the results of the simulation are plotted against the data taken in a period of 24 hours on Nov. 21, 2003. The peak bunch populations are similar to the values listed in Table 1 but the ratio of the currents was not maintained at low currents. Still, one can see that the agreement is surprisingly good. The beam-beam parameters in Fig 4 are estimated using Eq. 3, both in the measurement and the simulation. The beam-beam parameters differ between the positron and electron beams largely due to the violation of the energy transparency condition, $N_+\gamma_+ \neq N_-\gamma_-$. If we use Eq. 2 to compute the beam-beam parameter in the simulation, we have $\xi_{y,+} \approx \xi_{y,-} = 0.04$ at the peak currents.
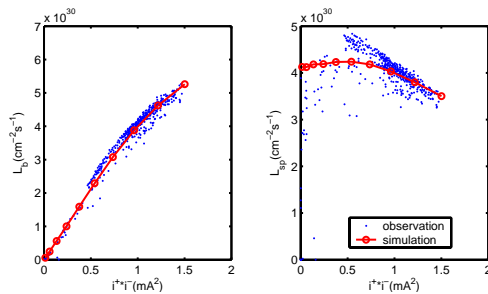

Figure 3: Luminosity and specific luminosity as a function of the product of beam currents.

Beam spectrum

The betatron spectra of both beams, measured at the peak currents, are shown in Fig 5. Both beam spectra in the horizontal plane are spread widely and nearly identical. These features are reproduced in the simulated spectra in Fig 6. Based on the simulation, we learn that the two peaks near the edge are σ and π modes respectively. These coherent dipole modes are excited because the horizontal
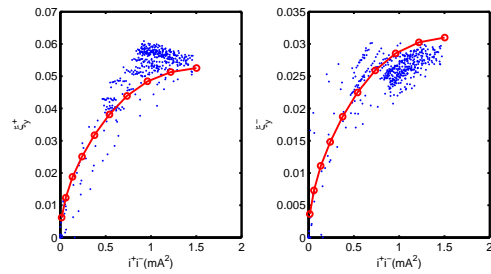

Figure 4: Vertical beam-beam parameter as a function of the product of beam currents.

tunes (Table 1) are very close to each other. Since the σ and π modes are identical for both beams, that explains the identical spectra in the horizontal plane. Knowing the Yokoya factor [9], we can estimate the beam-beam parameters from the separation between the σ and π modes. We have $\xi_{x,\pm} \approx 0.054$.

In the vertical plane, the tunes are sufficiently separated relative to the beam-beam parameter and therefore the σ and π modes are not excited. We see only positive tune shifts away from the machine tunes.
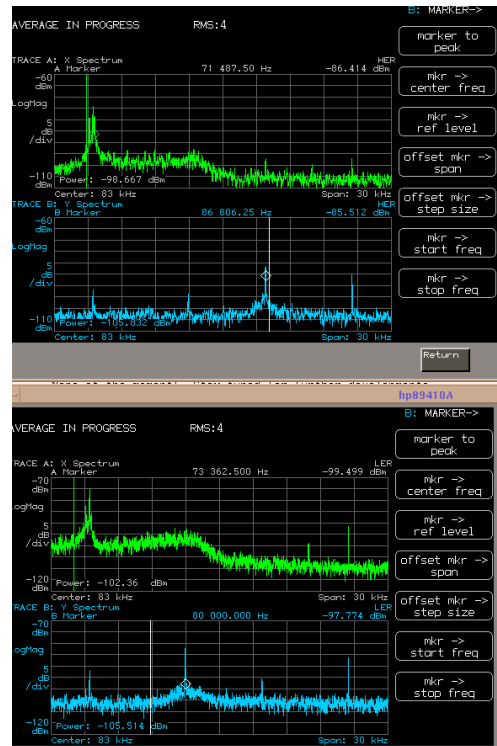

Figure 5: Measured colliding beam spectra at PEP-II a) e^- in x, b) e^- in y, c) e^+ in x, d) e^+ in y. The span is 30 kHz and $f_0 = 136.312$ kHz.

PARASITIC COLLISIONS

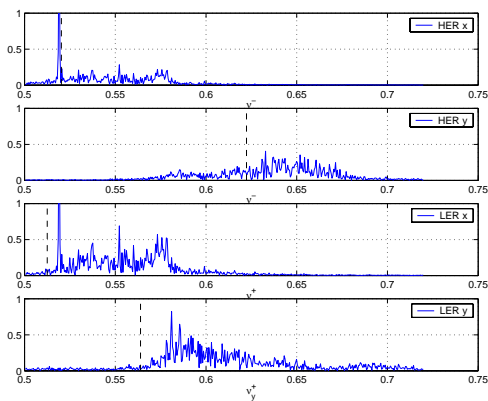In order to quantify the impact on the luminosity due to the parasitic collisions for the upgrade of PEP-II, we var-

Figure 6: Simulated colliding beam spectra at the peak operating currents. The dashed lines mark the machine tunes.

ied the beam separation Δx at the parasitic crossing points in the simulation. The fractional luminosity degradation relative to that without any parasitic collision is plotted in Fig. 7. For the nominal separation $\Delta x = 3.22$ mm, the reduction of the luminosity is about 7%. When the beams approach each other within 1.5 mm ($5\sigma_x^-$), the degradation is nearly 80% companied with a huge loss of particles. It is not clear why the reduction of luminosity has a quadratic functional dependence on the beam separation as shown in Fig. 7.
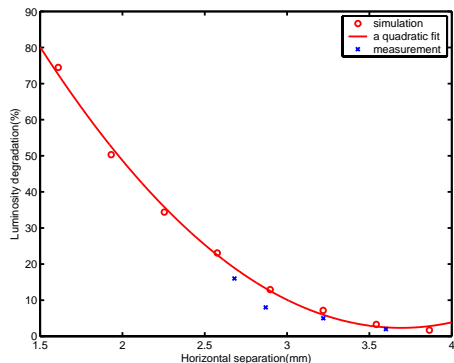

Figure 7: Luminosity degradation as a function of beam separation at the parasitic crossing.

In the dedicated experiment [7] illustrated in Fig. 8, the reduction due to the parasitic collision only ($\theta_c = 0$) is about 5% compared with 7% in the simulation.

LIFETIME

Beam lifetime were also recorded along with the luminosity on Nov. 21, 2003. The lifetimes measured every three minutes are plotted in Fig. 9. One can see that, as the beam currents approach their peak values, the beam lifetimes drop dramatically. This beam-beam lifetime defines the ultimate limit of the luminosity. That is why it is also called the second beam-beam limit.
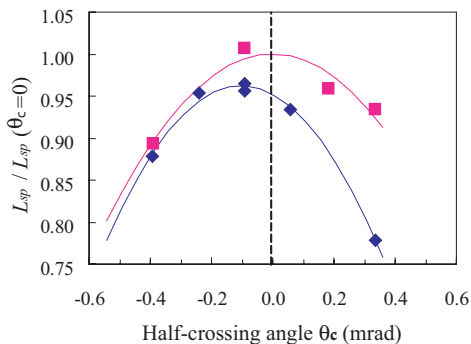

Figure 8: Normalized specific luminosity at a function of crossing angle with two different bunch patterns $s_b = 2s_{RF}$ (blue diamonds) and $s_b = 4s_{RF}$ (purple squares).
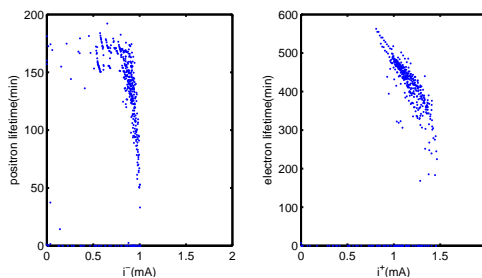

Figure 9: Measured lifetime as a function of the opposing beam current in a period of 24 hours during the regular operation.

Simulation

The beam-beam lifetime is determined by the dynamics in both the core and the tail of the beams, in contrast to the luminosity which is largely determined by the core of the beams. Traditionally [10], the tail distribution was studied using a strong-weak model and a linear map for the lattice, along with a leapfrog scheme to speed up the simulation. One drawback of that model is that the particles which are streamed out from the core to the tail of the beam, stay in the tail and never get lost because the beam-beam force becomes very weak at large amplitude. Therefore the lifetime is always infinite or is artificially determined by an imaginary physical aperture.

This situation can be improved by introducing a high-order map into the simulation. Since the nonlinear map defines the dynamic aperture in the machine, the particles reaching the tail of the beam will continue to migrate out due to the nonlinearity in the map. Therefore, the counting of the lost particles gives us an accurate calculation of beam-beam lifetime.

Here we continue to use the strong-weak model and assume the strong beam has a Gaussian distribution. Since each particle is essentially independent in this model, it is trivial to make the simulation parallel. For the Low Energy Ring of PEP-II, we found that an eighth order Taylor

map is adequate to reproduce the dynamic aperture calculated using the element-by-element tracking. In terms of the time spent on tracking particles, the five-slices beam-beam kick [6] is equivalent to a sixth order map with six variables. Each increasing order of the map reduces the speed by a factor of two. To make the map symplectic in tracking costs another factor of two.

20,000 macro particles were used to represent the positron beam and 120,000 turns (about 12 damping time) were tracked in each simulation. The number of lost particles were recorded in every turn. The loss rate stayed as a constant after three damping times. Lifetime was then calculated using the steady rate, $\tau = n_m T_0 N_{turns}/n_{loss}$, where n_m is the number of macro particles and T_0 is the revolution time. The accumulated distributions beyond three damping times are shown in Fig. 10. The beam-beam lifetime is infinite using the linear matrix and reduces to 16 minutes when the eighth-order map is used. However, the difference in luminosity is about 5%. The small difference provides us with a justification as to why the linear map can be used in strong-strong simulations.

Figure 11: Beam distributions at different tunes a) $\nu_x^+ = 0.5081, \tau = 1$ min, b) $\nu_x^+ = 0.5125, \tau = 16$ min, c) $\nu_x^+ = 0.5142, \tau = 100$ min, and d) $\nu_x^+ = 0.5152, \tau = \infty$ in the beam-beam simulation for PEP-II.

thing is that so many different measurements can be understood by the same simulation with the same input parameters. Most input parameters were independently measured with optical analysis.

In the beam-beam lifetime calculation, we have shown the importance of including the nonlinearity of the lattice in the simulation. With the high-order map, the lifetimes of the positron beam are simulated near the half integer resonance. The computed lifetimes qualitatively agree with the observations.

Acknowledgments

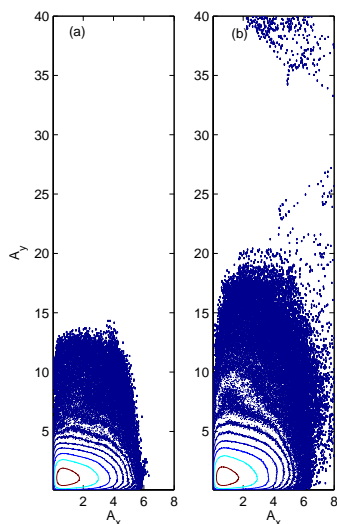We thank Yiton Yan for providing his Zlib for the map tracking.

Figure 10: Beam distributions using a) linear matrix or b) eighth-order Taylor map to represent the lattice of the Low Energy Ring ($\nu_x^+ = 0.5125$).

A tune scan with the eighth order map was performed to see the sensitivity of the beam-beam lifetime. The result is shown in Fig. 11. Incidentally, the lifetimes in the scan are very close to those near the edge of high beam current in Fig. 9. The result of the tune scan shows that there is a lifetime cliff near the half integer resonance. It was often seen in the PEP-II operating room where the operators tried to push to a high luminosity.

CONCLUSION

Many comparisons are made between the simulations and measurements at PEP-II. Given any specific comparison, the agreement is at the level of 10%. The important
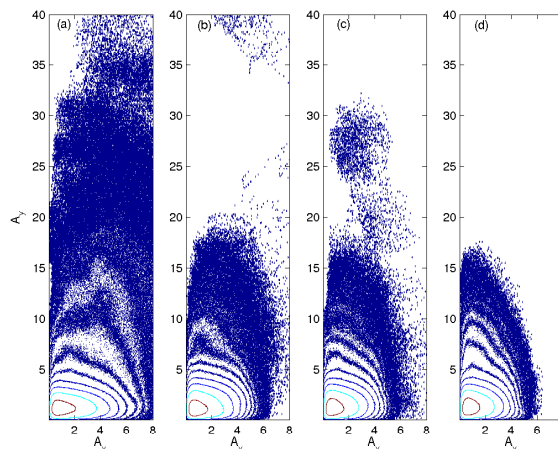
REFERENCES

[1] S. Krishnagopal and R. Siemann, Phys. Rev. Lett. **67**, 2461 (1991).

[2] S. Krishnagopal, Phys. Rev. Lett. **76**, 235 (1996).

[3] Y. Cai, A.W. Chao, S.I. Tzenov, and T. Tajima, Phys. Rev. ST Accel. Beams. **4**, 011001 (2001).

[4] K. Ohmi, Phys. Rev. E **62**, 7287 (2000).

[5] Y. Cai, SLAC-PUB-10674, August 2004, ICFA Beam Dyn. Newsletter, **34** 11, 2004.

[6] M. Bassetti and G. Erskine, CERN ISR TH/80-06 (1980).

[7] W. Kozanecki *et al.*, "Experimental Study of Crossing-Angle and Parasitic Crossing Effects at the PEP-II e^+e^- Collider," PAC'05, these proceedings.

[8] B. Viaud *et at*, "Measurement of the Luminous-Region Profile at the PEP-II IP, and Application to $e^\pm$ Bunch-Length Determination," PAC'05, these proceedings.

[9] K. Yokoya and H. Koiso, PA **27** 181 (1990).

[10] T. Chen, J. Irwin, and R. Siemann, Phys. Rev. E **49** 2323 (1994).